

# Topological defect motifs in two-dimensional Coulomb clusters

A Radzvilavičius and E Anisimovas

Department of Theoretical Physics, Vilnius University, Saulėtekio 9, LT-10222  
Vilnius, Lithuania

**Abstract.** The most energetically favourable arrangement of low-density electrons in an infinite two-dimensional plane is the ordered triangular Wigner lattice. However, in most instances of contemporary interest one deals instead with finite clusters of strongly interacting particles localized in potential traps, for example, in complex plasmas. In the current contribution we study distribution of topological defects in two-dimensional Coulomb clusters with parabolic lateral confinement. The minima hopping algorithm based on molecular dynamics is used to efficiently locate the ground- and low-energy metastable states, and their structure is analyzed by means of the Delaunay triangulation. The size, structure and distribution of geometry-induced lattice imperfections strongly depends on the system size and the energetic state. Besides isolated disclinations and dislocations, classification of defect motifs includes defect compounds — grain boundaries, rosette defects, vacancies and interstitial particles. Proliferation of defects in metastable configurations destroys the orientational order of the Wigner lattice.

PACS numbers: 61.46.Bc, 02.70.Ns, 61.72.Bb

## 1. Introduction

The most energetically favourable arrangement of low-density electrons in an infinite two-dimensional plane is the ordered triangular Wigner lattice [1, 2] where each electron is surrounded by six equidistant nearest neighbours. However, in most instances of contemporary interest one deals instead with finite clusters of strongly interacting particles localized in potential traps. For example, extensively studied realizations of finite-size two-dimensional Wigner crystallites are created by trapping charged micrometric particles formed in the complex plasma environment [3]. Confined geometries inevitably lead to deviations from the perfect triangular structure.

Presence of lattice imperfections plays a key role in determination of physical properties of both macroscopic [4] and low-dimensional mesoscopic systems. It has been argued that lattice faults are important in the shape changing processes during the maturation of capsids of spherical viruses [5], cell division, and growth of bacterial surface layers [6]. Intrinsic defects have a major impact on the collective particle motion and the inhomogeneous melting of two-dimensional Coulomb clusters in circular confinement [7] and straight narrow channels [8].

The topological charge — also known as the disclination charge — of a site in a distorted lattice is defined as  $Q = \tilde{C} - C$ ; here  $C$  is the actual coordination number (the number of nearest neighbours) and  $\tilde{C}$  is the reference value pertaining to the perfect lattice. For sites that belong to the bulk of the cluster  $\tilde{C} = 6$ , while for those situated on the edge  $\tilde{C} = 4$ . The topological charges of all sites in a two-dimensional cluster must sum up to six, a topological invariant due to the Euler's theorem [9].

In a recent work [10] topological defects and defect complexes were investigated in the Thomson model [11], featuring a fixed number of particles moving on the surface of a sphere and interacting through repulsive Coulomb forces. In a quasi-three-dimensional geometry defined by the spherical surface the total disclination charge must equal twelve [12]. It was shown that in systems consisting of 400 particles or more, isolated defects cost too much strain energy, and thus, various defect complexes are formed. The most intriguing of the lot are the so-called *rosette* defects consisting of a central five-coordinated site (topological charge  $Q = 1$ ) surrounded by a layer of five seven-coordinated sites ( $Q = -1$ ), and a further layer of five five-coordinated sites. The total disclination charge of this compound is  $Q_{\text{net}} = 1$ . Thus, highly symmetric configurations with 12 rosettes arranged on a sphere must be possible and were indeed reported in reference [10].

The purpose of the present paper is a comprehensive study and classification of topological defects in a two-dimensional Coulomb cluster — a mesoscopic system, known for its applicability to a broad range of experimental problems, namely, the distribution of electron islands on the surface of liquid helium [2, 13], electrons in semiconductor quantum dots [14] and charged micrometric spheres in the complex plasma environment [3, 15]. The system consists of a given number of identical charged particles confined by an isotropic parabolic potential trap. The confinement gives rise to the presence

of topological defects. The number, structure and distribution of defects, or defect complexes, strongly depends on the system size and its energetic state.

As a matter of fact, in large Coulomb clusters an exponentially large number of stable configurations are possible [16]. The one with the lowest energy is called the ground state and is, of course, the most special and interesting configuration. However, metastable states are also realized in experiments [17] and should not be neglected. Therefore, we do not restrict our attention to the ground states but investigate the whole spectrum, mostly focusing on its low-energy part.

We use the term *low-energy states* to refer to the states whose energies fall within the bottom 20% of the energy interval covered by all discovered metastable states.

The presence of a large number of competing metastable states is also a computational issue. Various methods have been tried striving to locate the ground state as well as metastable configurations of large clusters. Simulated annealing [18], genetic algorithms [12] and basin hopping [19] are a few significant examples. In the present work, we rely on the recently proposed minima hopping method [20]. This algorithm is designed to avoid revisiting already known configurations and employs low-energy molecular dynamics escape trajectories to reach neighbouring energy minima from a given one. The minima hopping method was shown to be efficient in locating ground states of complex molecular systems [21], and with the present contribution we test its performance on strongly coupled Coulomb systems.

The paper is organized as follows. In Section 2, we introduce the model and the computational scheme. The three subsections of section 3 are devoted to discussion and classification of the obtained defect compounds and their impact on the orientational order of the Wigner lattice. We end with a concluding section 4.

## 2. Model system and computational approach

The model system consists of  $N$  identical particles of mass  $m$  and electrostatic charge  $q$ , restricted to move in a two-dimensional plane and laterally confined by a circular parabolic potential. The total potential energy of the system is given by

$$U(\mathbf{r}_1, \dots, \mathbf{r}_N) = \sum_{i=1}^N \frac{1}{2} m \omega_0^2 \mathbf{r}_i^2 + \sum_{i>j}^N \frac{q^2}{r_{ij}}. \quad (1)$$

Here,  $\mathbf{r}_i$  is a two-dimensional vector denoting the position of the  $i$ -th particle and  $r_{ij} = |\mathbf{r}_i - \mathbf{r}_j|$  is the distance between two of them. The first term of (1) represents the parabolic confinement with the characteristic frequency  $\omega_0$ , while the second term corresponds to the Coulomb interparticle repulsion. Introducing the units of length  $r_0 = (q^2/m\omega_0^2)^{1/3}$  and energy  $E_0 = q^2/r_0$ , we rewrite the potential energy (1) in a simple dimensionless and parameter-free form

$$U(\mathbf{r}_1, \dots, \mathbf{r}_N) = \sum_{i=1}^N \frac{1}{2} \mathbf{r}_i^2 + \sum_{i>j}^N \frac{1}{r_{ij}}. \quad (2)$$

To find the low-energy stable states of the cluster, we use the minima hopping algorithm [20]. Since application of this algorithm is novel in this context, we begin with a brief outline.

Initially, the system is placed into one of the known minima and the algorithm starts by performing a short molecular dynamics simulation that attempts to escape from the basin of attraction of the current minimum. The particles are assigned random velocities according to the Maxwell distribution scaled in such a way that their total kinetic energy adds up to the current value of  $E_{\text{kin}}$ , a dynamically adjustable simulation parameter. The molecular dynamics simulation proceeds keeping track of the instantaneous value of the potential energy, and is stopped immediately after its  $\text{md}_{\text{min}}$ -th minimum along the simulation path is reached. In the simplest version of the algorithm, the parameter  $\text{md}_{\text{min}}$  is set to unity, that is, the nearest minimum is sought. However, one may often wish to skip some minima along the trajectory, and such an opportunity is provided by using larger values of  $\text{md}_{\text{min}}$ .

Once the molecular dynamics simulation is stopped, the geometry minimization takes over and the system is forced to roll down towards the closest minimum. This step is accomplished by a combination of the steepest descent and Newton's optimization techniques.

There are three possible outcomes of the described simulation. If the kinetic energy  $E_{\text{kin}}$  is insufficient to overcome the surrounding potential barriers and/or the parameter  $\text{md}_{\text{min}}$  is not large enough to find a low-energy escape path, the system rolls back to the same minimum. In the second case, the new minimum turns out to be visited previously. If any of these two outcomes is reached, the kinetic energy of the system is increased by a respective factor  $\beta_1$  or  $\beta_2$  (see below) and a new more vigorous attempt is launched from the same minimum. The third and most desirable case is realized when the obtained minimum is a new one and has not been visited previously.

To introduce a preference for steps that reduce the total potential energy, the new configuration is accepted only if the increase in the potential energy does not exceed the threshold value  $E_{\text{diff}}$ , another dynamically adjustable parameter. If the newly found minimum is accepted, the kinetic energy of the system  $E_{\text{kin}}$  is lowered and the following cycle is started from the new minimum.

The simulation is stopped after  $E_{\text{kin}}$  increases significantly. This happens when the simulation is unable to produce any new minima for a long time, which implies that the lowest minima have been found.

The behaviour of the energies  $E_{\text{kin}}$  and  $E_{\text{diff}}$  is governed by five control parameters. The factors  $\alpha_1$  and  $\alpha_2$  determine how fast  $E_{\text{diff}}$  is increased (decreased) after a new minimum is rejected (accepted). The factors  $\beta_1$ ,  $\beta_2$  and  $\beta_3$  multiply the kinetic energy  $E_{\text{kin}}$  according to the outcome of an escape attempt, and must be chosen close to unity in order to sample the phase space thoroughly. In our simulations we follow [20] and use  $\beta_1 = \beta_2 = 1/\beta_3 = 1.05$  and  $\alpha_1 = 1/\alpha_2 = 1.02$ . Finally,  $\text{md}_{\text{min}}$  determines the number of minima along the molecular dynamics path before the geometry relaxation takes over.

**Table 1.** The total number of minima hopping steps  $n_{\text{steps}}$ , the number of visited minima  $n_{\text{min}}$  and the trajectory-averaged kinetic energy  $\langle E_{\text{kin}} \rangle$  before the ground state is reached for different values of the control parameter  $\text{md}_{\text{min}}$  in the 85-particle cluster.

| $\text{md}_{\text{min}}$ | $n_{\text{min}}$ | $n_{\text{steps}}$ | $\langle E_{\text{kin}} \rangle$ |
|--------------------------|------------------|--------------------|----------------------------------|
| 1                        | 11.94            | 204.34             | 18.19                            |
| 10                       | 12.05            | 135.30             | 7.51                             |
| 20                       | 11.59            | 124.69             | 6.30                             |
| 25                       | 10.27            | 104.20             | 5.06                             |
| 35                       | 9.62             | 96.65              | 4.55                             |
| 50                       | 9.44             | 93.14              | 4.03                             |
| 75                       | 9.01             | 86.44              | 4.24                             |
| 90                       | 8.58             | 80.86              | 3.80                             |

The success of the algorithm is based on the validity of the Bell-Evans-Polanyi principle [20] which states that highly exothermic chemical reactions have a low activation energy. In other words, low-energy local minima are more likely to be located behind low potential barriers, and this is the reason to keep the kinetic energy as low as possible. Having performed some test runs we verified that the minima hopping algorithm never fails to find the true ground state of a three-dimensional Coulomb cluster with  $N \leq 170$  particles and the Thomson problem with  $N \leq 190$ .

We further investigated the performance of the minima hopping algorithm in the case of a two-dimensional 85-particle cluster. This cluster has a symmetric ground state that controls a rather small basin of attraction and 177 metastable states known from the previous work [16]. Thus, the search for the ground state is not a simple task.

The algorithm starts at a randomly chosen initial minimum and runs until the true ground state is reached. To collect reliable statistics, the whole simulation is repeated 500 times. The total number of the algorithm steps  $n_{\text{steps}}$  needed to reach the ground state strongly depends on the value of  $\text{md}_{\text{min}}$  and correlates with the average kinetic energy of the system  $\langle E_{\text{kin}} \rangle$  during the course of the simulation. From table 1 we observe that larger values of the parameter  $\text{md}_{\text{min}}$  result in lower values of  $\langle E_{\text{kin}} \rangle$  and a significant decrease of the total number of simulation steps.

Higher values of  $\text{md}_{\text{min}}$  are beneficial as they allow the system to oscillate more frequently within the area of the current basin or jump over a few barriers and thus increases chances to find low-energy escape trajectories. Higher values of  $\text{md}_{\text{min}}$  also lead to a slightly lower number of minima  $n_{\text{min}}$  visited before the ground state is found. These observations confirm the validity of the Bell-Evans-Polanyi principle in Coulomb systems. On the other hand, large values of  $\text{md}_{\text{min}}$  also increase the total computing time which strongly depends on the length of molecular dynamics trajectories. Therefore, in the bulk of our calculations we used moderate values  $\text{md}_{\text{min}} = 2$  or  $3$ .

### 3. Defect motifs in two dimensions

In this section, we report the results of the minima hopping simulations of two-dimensional classical Coulomb clusters in the range of sizes  $1 \leq N \leq 1000$  as well as a few cluster configurations of larger sizes:  $N = 2000$ ,  $3000$  and  $4000$ . The structure of the cluster and, consequently, the nature and distribution of topological defects strongly depends on the system size. Various aspects of topological defects of relatively small clusters have been considered before [9, 22, 23]. Our aim is a comprehensive study of a broad range of sizes, and most importantly, classification of the determined structures some of which were previously not seen in two-dimensional systems.

The analysis of the structure of a Coulomb cluster starts by determining the coordination number (the number of nearest neighbours) for all particles in the cluster. By definition, two particles are considered nearest neighbours if they are connected by a link in the Delaunay triangulation [24], which provides an unambiguous algorithm to construct a net of triangles given a set of points on a plane. Figure 1 provides several examples of triangulated cluster structures. The symbols used in our figures are as follows: Gray lines depict the triangulation net, and ordinary six-coordinated vertices are shown by gray circles. Red triangles mark positive disclinations, that is, particles missing a neighbour; likewise blue squares (absent from figure 1) mark negative disclinations. Incidentally, the Delaunay triangulation is dual to the Voronoi construction [24] which is also often used in similar contexts [22, 23, 25].

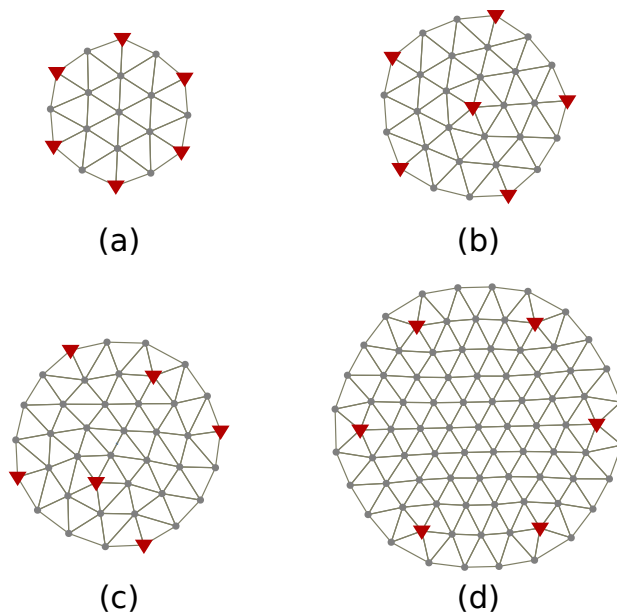


**Figure 1.** Configurations of Coulomb clusters featuring six isolated disclinations denoted by red triangles: (a) the ground state of 19-particle cluster, (b) a metastable state of a 31-particle cluster, (c) a ground state of a 40-particle cluster, and (d) the ground state of a 85-particle cluster.

Distribution of defects in a parabolic confinement is by large determined by a

conflict between the circular boundary and the bulk-like interior where a hexagonal lattice is preferred. Small clusters ( $N \lesssim 70$ ) have no bulk and exhibit a shell structure defined by the circular symmetry of the confinement. A large fraction of the particles is located on the edge. Hence, small clusters often satisfy the Euler's theorem solely by the presence of edge disclinations, such as the 19-particle cluster shown in figure 1 (a), while the distribution of defects is sensitive to addition or subtraction of a single particle. Defect complexes are also frequently found in the interior, however, these defects are also the consequence of the well expressed shell structure and thus should not be interpreted as perturbations of a hexagonal lattice.

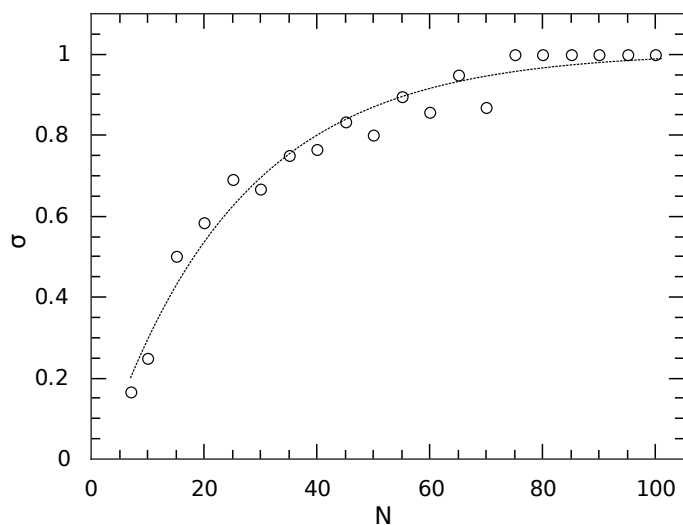


**Figure 2.** Distribution of particles on the periphery of the ground-state clusters. The ratio of the number of particles in the outermost shell to the number of particles in second farthest shell,  $\sigma$ , is plotted as a function of the system size  $N$ . The dotted line is drawn to guide the eye.

Figure 2 shows that the number of particles in the two outermost shells equalizes for clusters larger than  $N \approx 70$ . Once this critical size is exceeded, a well-defined bulk develops, and only two or three external shells are nearly circular and contain approximately the same number of particles. In most cases, the defects move into the transition region between the circular outer part and the triangular interior. Six groups of defects, located at the corners of a hexagon can often be distinguished [23], and the size and composition of the observed defect structures become insensitive to the addition of a single particle to the cluster.

### 3.1. Defect chains

The predominant defect structure in two-dimensional Coulomb clusters is a defect chain consisting of alternating positive and negative disclinations, that is, five- and seven-coordinated vertices. In many (but not all) cases the number of positive disclinations

in such a chain equals the number of negative disclinations plus one. Thus, the net topological charge of the chain equals  $Q_{\text{net}} = 1$ .

A trivial case of this class is a chain of length one, that is, a single isolated defect.

**Isolated positive disclinations** are frequently observed in relatively small systems. The presence of six  $Q = 1$  defects is the simplest way to satisfy the Euler's theorem, however, stable configurations with six isolated disclinations, are not very common. A few notable high-symmetry examples are shown in figure 1. Here we show two structures of  $C_6$  symmetry — the ground states of  $N = 19$  and  $N = 85$  particle clusters in panels (a) and (d). Structures of  $C_5$  symmetry are also possible, for example, the ground state of a 16-particle cluster (not shown) and a metastable state of a 31-particle cluster shown in panel (b). Figure 1 (c) shows an example of a low-symmetry configuration — the ground state of a 40-particle cluster.

**Isolated negative disclinations** are observed in some metastable configurations of small clusters, for example with  $N = 38, 40, 60,$  and  $80$ . This defect, however, is always accompanied by a positive disclination or other defects in the close neighbourhood.

As the number of particles increases, isolated disclinations tend to disappear. Free disclinations are only rarely observed in low-energy states of clusters with the number of particles close to  $N \approx 300$  and are not observed at all in larger systems.

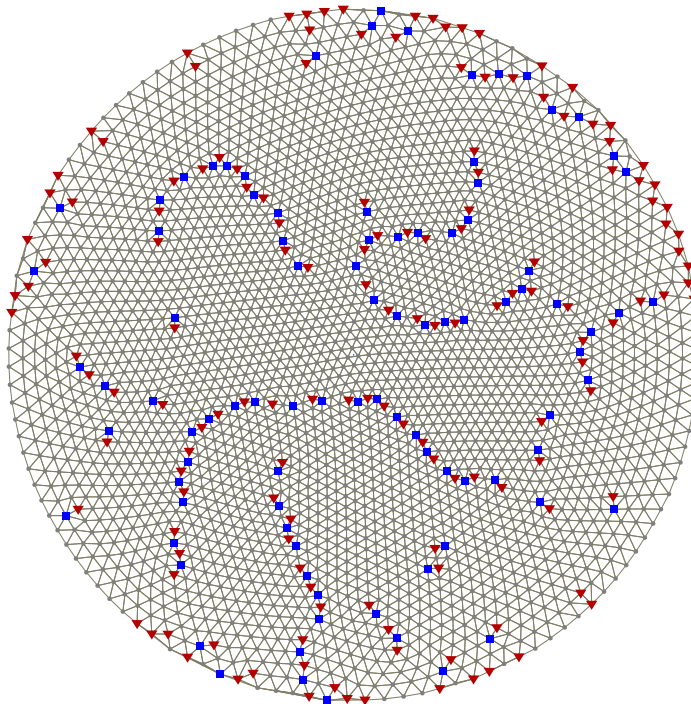


**Figure 3.** Metastable state of a 3000-particle Coulomb cluster. Long defect chains divide the interior into zones with different lattice orientation. Configurations of other investigated systems with several thousand particles are qualitatively similar.

**A dislocation** is a topologically neutral defect, a pair of adjacent five- and seven-coordinated vertices, which may be regarded as a primitive chain of length two.



Dislocations reduce strain induced by disclinations [9]. The number of free dislocations in general increases with the energy of metastable state. Numerous dislocations can be seen in figure 3 which shows a high-energy metastable state of a 3 000-particle Coulomb cluster.

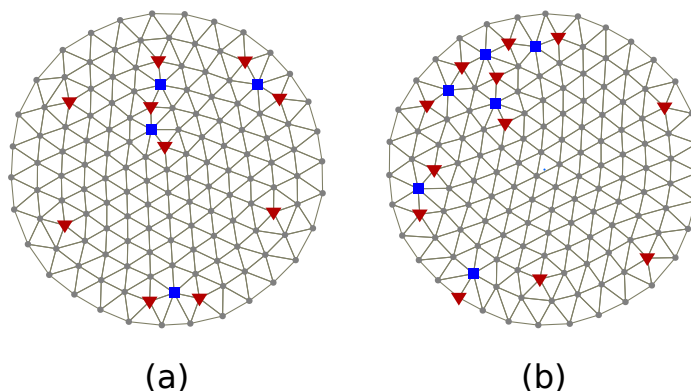


**Figure 4.** Ground (a) and high-energy metastable (b) states of a 143-particle cluster. In the ground state, three disclinations, two extended dislocations and short grain boundary occupy the six corners of a hexagon. The hexagonal structure is lost in metastable states.

In larger systems, longer chains of defective vertices become energetically favourable. **An extended dislocation**, also referred to as a scar [10], is a negative disclination flanked by two positive disclinations. It has the shape close to that of the  $\text{H}_2\text{O}$  molecule [see figure 4 (a)] and the net topological charge  $Q_{\text{net}} = 1$ . This structure may be regarded as a rudimentary grain boundary. Scars are often present in metastable states of small clusters and ground states in the size range of  $N \approx 100 \dots 460$  particles. Configurations with six isolated extended dislocations at the six corners of hexagon are observed at some values of  $N$ ; a few examples are  $N = 200, 210, 250$ , and  $N = 291$ . In larger clusters, such as the near-ground-state of  $N = 560$  system, scars appear in complexes with additional dislocations.

**Length-5** grain boundaries, consisting of alternating three  $Q = 1$  and two  $Q = -1$  vertices appear in metastable states of small clusters. Later, these defect chains replace single disclinations or extended dislocations in some of the six defect groups of large clusters. An illustrative example with all three types of defects is given in figure 4. As the number of particle grows, the number and length of the grain boundaries in the low-energy metastable states on the average increases. However, the growth of the number of defective vertices is not uniform. In many cases of large clusters, at least one of these defect chains points radially towards the center of the cluster; the others separate the inner region from the circular part of the cluster (see figure 5). Some of the grain boundaries are also accompanied by a few five- and seven-coordinated vertex pairs.

**Lengthy grain boundaries** and neutral disclination-dislocation chains appear in the interior of high-energy metastable states of large systems. They divide the inner

part of the cluster into distinct zones with different orientations of crystallographic axes. Extremely long defect chains (20 vertices and more) are present in metastable states of crystals with a few thousand particles shown in figure 3, giving rise to polycrystalline order.

### 3.2. Complex structures

A number of defect structures do not follow the general shape of a chain. The first of these complex motifs is a **twin grain boundary** with a local mirror line. The twin grain boundary consists of two negative disclinations, sharing a common triangulation edge, and three positive disclinations on the periphery. Thus, the net topological charge of the structure is  $Q_{\text{net}} = 1$ . Twin grain boundaries have been reported in the low-energy minima of the Thomson model [26] but were not discussed in 2D Coulomb systems.

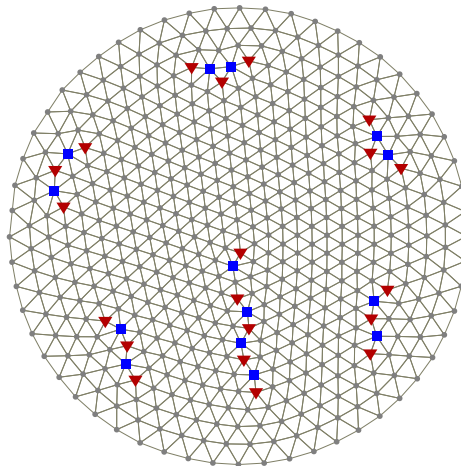


**Figure 5.** Low-energy metastable state of 520-particle two-dimensional Coulomb cluster shows a typical defect distribution of this size range. Two twin grain boundaries, three length-5 grain boundaries and one radial length-7 defect chain, screened by an additional dislocation are located in the corners of a hexagon.

Twin grain boundaries first appear in metastable states of relatively small clusters ( $N = 90$  is one of the examples), and then among the groups of defects situated in the corners of a hexagon in larger systems as seen in figure 5. Some twin grain boundaries in large crystals are extended by a few additional pairs of  $Q = \pm 1$  defects, or are screened by neighbouring dislocations (see figure 6).

A unique **rosette** defect of pentagonal symmetry is present in some of the low-energy metastable states of large clusters ( $N > 600$ ). A rosette consists of a central positive disclination surrounded by five negative disclinations alternating with five positive disclinations. The net topological charge of this complex equals  $Q_{\text{net}} = 1$ . Highly symmetric configurations of 12 rosettes were previously observed in low-energy states of spherical Thomson clusters [10]. In two-dimensional Coulomb systems rosettes were not reported before, and we observe at most one rosette per cluster. Further

simulations of larger crystals would be needed to investigate, if the presence of multiple rosettes is ever possible.

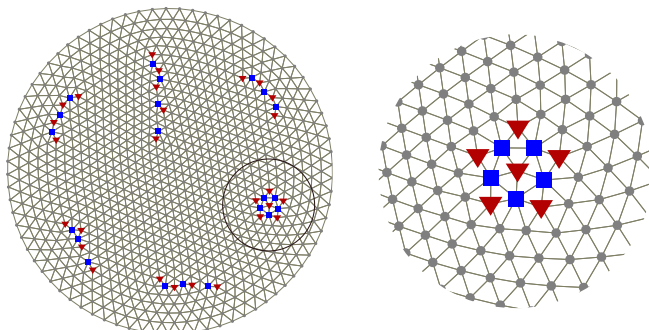


**Figure 6.** Rosette defect in low-energy metastable state of a 1 000-particle cluster.

A few classes of cyclic defect configurations are observed in high-energy metastable states of large systems and are shown in figure 7. There are two triangular structures composed of three positive and three negative disclinations, and a rhombus-shaped structure consisting of two  $Q = 1$  vertices accompanied with two  $Q = -1$  vertices. Two types of triangular structures are present: Panel (a) shows the smaller of the two, with three seven-coordinated particles moved close to the center of the motif, and panel (b) presents the larger structure which encircles a six-coordinated particle. All these complexes are topologically neutral and do not change the global hexagonal symmetry of the lattice. However, they do change the local density of the particles — the complex shown in figure 7 (a) is a vacancy, whereas the ones seen in figure 7 (b) and (c) are interstitial particles [27].

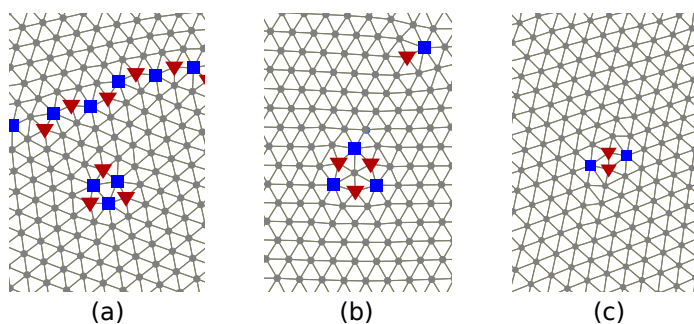


**Figure 7.** Topologically neutral complexes: (a) a triangle-shaped vacancy in the core of high energy metastable state of  $N = 900$  cluster situated close to a long grain boundary, (b) an interstitial defect in the inner region of  $N = 690$  Coulomb system, and (c) a rhombus-shaped interstitial in a metastable state of a  $N = 604$  particle cluster.

### 3.3. Bond-orientational order

As the energy of a metastable state increases, the average number of defective vertices grows [23] and the hexagonal symmetry of the defect clustering positions is lost. Topological defects are observed both in the interior and on the edge of a cluster. Lattice imperfections tend to form long chains and asymmetric complexes that heavily distort the triangular structure. To quantify the loss of structural order in high-energy metastable states, we evaluate the site-averaged complex bond-orientational order (BOO) parameter. For a single site, the BOO parameter is defined as [28]

$$\Psi_6 = \frac{1}{C} \sum_{k=1}^C \exp(i6\theta_k). \quad (3)$$

Here,  $\theta_k$  is the angle of the vector drawn from the particle in question to the  $k$ -th of its nearest neighbours. An ordered site on a perfect triangular lattice has  $|\Psi_6| = 1$ . A slightly distorted site with six nearest neighbours and low strain usually has  $|\Psi_6| > 0.4$ , whereas a heavily distorted site with five or seven neighbours has  $|\Psi_6| < 0.4$  [8]. To evaluate the degree of orientational order in the core of a cluster, we average the absolute value of the BOO parameter  $\Psi_6$  over all sites except those located within three outermost shells.

The lowest-energy configurations of large clusters correspond to the bond-orientational order parameter within the range  $|\Psi_6| \approx 0.66 \dots 0.80$ , depending on the actual size and distribution of defects with respect to the center of the cluster. For example, a low-energy state of the 520-particle crystal shown in figure 5 includes a radially oriented compound of a length-7 grain boundary and a nearby dislocation, and thus has a low value of  $|\Psi_6| = 0.66$ . On the other hand, the longest defect chain in the system with  $N = 550$  particles is composed of only five defective vertices. The core of the cluster is defect free, and hence, the orientational order is relatively high,  $|\Psi_6| = 0.8$ .

The dependence of the averaged BOO parameter  $|\Psi_6|_{\text{avg}}$  on the energy of the metastable state is shown in figure 8 for  $N = 1000$ . We see, that at low energies the values of the BOO parameter indicate ordered states of the lattice ( $\Psi_6 \approx 0.7$ ). The value of the order parameter is subject to substantial fluctuations, however, the general trend is clearly visible: As the energy of the state increases, the order is gradually lost. The values of BOO drop as low as  $|\Psi_6|_{\text{avg}} \approx 0.2$  for metastable states with the highest energies. These configurations have a large number of long grain boundaries at the core of the cluster that separate regions of different local orientation of the lattice.

We observe that metastable states of large clusters, different in size or orientation of only a few defects, are very close in their energy. As a notable example we consider a metastable state of  $N = 1000$  particle system and energy  $E = 103\,457.1505$ . A slight change of the orientation of a defect pair near the extended dislocation changes the energy of the state by  $\Delta E = 0.0002$ . Likewise, as the disclination screened by two dislocations transforms into length-5 grain boundary, the energy of the system increases by only 0.0001.

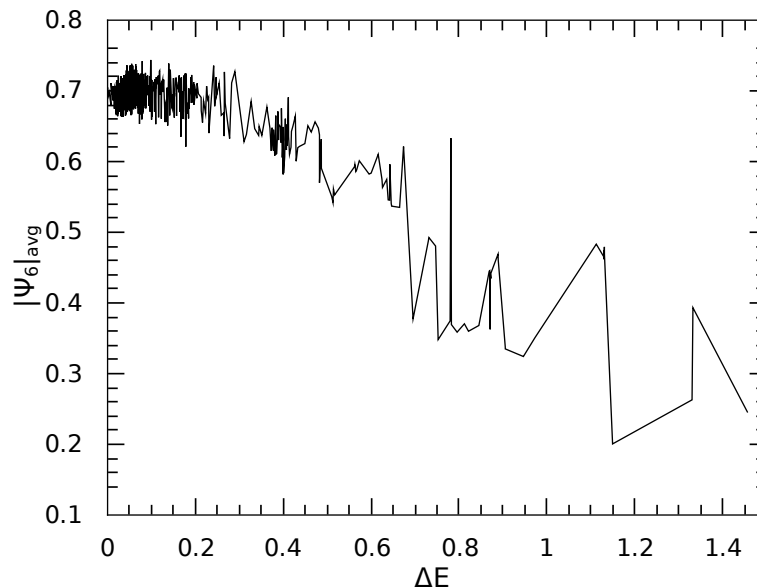


**Figure 8.** Absolute value of bond-orientational order parameter  $\Psi_6$  averaged over the sites at the core of the 2D Coulomb cluster with  $N = 1000$  particles versus the relative energy of metastable states. Here,  $\Delta E$  is the energy measured from the lowest found state.

#### 4. Conclusion

We performed minima hopping simulations of isotropic two-dimensional Coulomb clusters in order to study the distribution and transformations of intrinsic topological defects in low-energy stable configurations. We conclude, that with properly chosen values of control parameters, the minima hopping technique is an efficient and fast method to locate the candidates for the ground states in strongly coupled Coulomb systems.

The distribution and size of the geometry-induced defects strongly depends on the system size and its energetic state. As the cluster size increases, free disclinations are gradually replaced by more energetically favourable extended dislocations and grain boundaries of non-uniformly increasing length. A novel rosette defect, previously seen only in metastable states of a quasi-three-dimensional Thomson model, is shown to be present in low-energy states of large clusters. However, we observe only one rosette per crystal. Cyclic defects — triangle and rhombus-shaped vacancies and interstitial particles — are observed in high-energy metastable states of two-dimensional Coulomb systems.

As the energy of metastable states grows, the orientational order at the core of large clusters is lost due to the appearance of elongated grain boundaries and increased concentration of dislocations.

## Acknowledgments

This research was funded by a grant No. MIP-79/2010 from the Research Council of Lithuania.

## References

- [1] Wigner E 1934 *Phys. Rev.* **46** 1002  
Gann R C, Chakravarty S and Chester G V 1979 *Phys. Rev. B* **20** 326  
Grimes C C and Adams G 1979 *Phys. Rev. Lett.* **42** 795
- [2] Crandall R S and Williams R 1971 *Phys. Lett. A* **34** 404
- [3] Bonitz M, Henning C and Block D 2010 *Rep. Prog. Phys.* **73** 066501
- [4] Ashcroft N W and Mermin N D 1976 *Solid State Physics* (Fort Worth: Saunders College Publishing)
- [5] Iorio A and Sen S 2008 *Cent. Eur. J. Biol.* **3** 380
- [6] Pum D, Messner P and Sleytr U B 1991 *J. Bacteriol.* **173** 6865
- [7] Lai Y-J and I L 2001 *Phys. Rev. E* **64** 015601
- [8] Liu K-A and I L 2010 *Phys. Rev. E* **82** 041504
- [9] Koulakov A A and Shklovskii B I 1998 *Phys. Rev. B* **57** 2352
- [10] Wales D J, McKay H and Altschuler E L 2009 *Phys. Rev. B* **79** 224115
- [11] Thomson J 1904 *Philos. Mag.* **7** 237
- [12] Morris J R, Deaven D M and Ho K M 1996 *Phys. Rev. B* **53** 1740
- [13] Rousseau E, Ponarin D, Hristakos L, Avenel O, Varoquaux E and Mukharsky Y 2009 *Phys. Rev. B* **79** 045406
- [14] Filinov A V, Bonitz M and Lozovik Yu E 2001 *Phys. Rev. Lett.* **86** 3851
- [15] Juan W-T, Huang Z-H, Hsu J-W, Lai Y-J and I L 1988 *Phys. Rev. E* **58** 6947
- [16] Radzvilavičius A and Anisimovas E 2011 *J. Phys.: Condens. Matter* **23** 075302
- [17] Kählert H, Ludwig P, Baumgartner H, Bonitz M, Block D, Käding S, Melzer A and Piel A 2008 *Phys. Rev. E* **78** 036408
- [18] Press W H, Teukolsky S A, Vetterling W T and Flannery B P 2007 *Numerical Recipes: The Art of Scientific Computing* 3rd edn (Cambridge: Cambridge University Press)
- [19] Wales D J, Doye J P K 1997 *J. Phys. Chem. A* **101** 5111
- [20] Goedecker S 2004 *J. Chem. Phys.* **120** 9911
- [21] Schönborn S E, Goedecker S, Roy S and Oganov A R 2009 *J. Chem. Phys.* **130** 144108
- [22] Lai Y-J and I L 1999 *Phys. Rev. E* **60** 4743
- [23] Kong M, Partoens B and Peeters F M 2003 *Phys. Rev. E* **67** 021608
- [24] Preparata F P and Shamos M I 1985 *Computational Geometry: An Introduction* (Berlin: Springer) ch 5
- [25] Mughal A and Moore M A 2007 *Phys. Rev. E* **76** 011606
- [26] Wales D J and Ulker S 2006 *Phys. Rev. B* **74** 212101
- [27] Cândido L, Phillips P and Ceperley D M 2001 *Phys. Rev. Lett.* **86** 492
- [28] Halperin B I and Nelson D R 1978 *Phys. Rev. Lett.* **41** 121